arXiv:1603.06672v2 [astro-ph.CO] 16 Sep 2016

ON THE UNIVERSALITY OF THE BOUND-ZONE PECULIAR VELOCITY PROFILE

Jounghun Lee

Astronomy Program, Department of Physics and Astronomy, Seoul National University, Seoul 08826, Republic of Korea

jounghun@astro.snu.ac.kr

ABSTRACT

A numerical evidence for the universality of the bound-zone peculiar velocity profile in a ΛCDM universe is presented. Analyzing the dark matter halo catalogs from the Millennium-II simulation, we determine the average peculiar velocity profiles of the objects located in the bound zones around massive group-size halos at various redshifts and compare them to an analytic formula characterized by two parameters, the amplitude and slope of the profile. The best-fit values of the two parameters are found to be robust against the changes of the mass scales and the key cosmological parameters. It is also found that the amplitude and slope parameters of the bound-zone peculiar velocity profile are constant but only in the limited ranges of redshifts. In the dark matter dominated epoch corresponding to $z > 0.6$ the two parameters have constant values. In the transition period corresponding to $0.2 \leq z \leq 0.6$ when the density of Λ begins to exceed that of dark matter the two parameters grow almost linearly with redshifts. At later epochs $z < 0.2$ when the Λ-domination prevails the two parameters regain constancy settling upon higher constant values. Noting that the length of the transition period depends on the amount of Λ and speculating that the linear evolution of the profile with redshifts in the transition period is a unique feature of the Λ-dominated universe, we suggest that the redshift evolution of the bound-zone peculiar velocity profile should be a powerful local discriminator of dark energy candidates.

Subject headings: cosmology:theory — large-scale structure of universe

1. INTRODUCTION

In the field of cosmology, the turn-around radius of a bound object is rather a classical concept, defined as the radius that an overdense region of which the object has condensed out

must have had at the moment when a perfect balance between the attraction of its self-gravity and the repulsion of the expanding spacetime was struck prior to the occurrence of its gravitational collapse (Gunn & Gott 1972). The very definition of the turn-around radius implies that it must be sensitively dependent upon the amount of dark matter, dark energy and the nature of gravity (see, e.g., Lahav et al. 1991; Barrow & Saich 1993; Mota & van de Bruck 2004; Borisov et al. 2012; Fan et al. 2015).

Until recently, however, its importance and power as a cosmological discriminator has not been well recognized mostly because of the concern over the practical difficulty to measure it from observations. Unlike the viral radius of a bound object that is a nonlinear quantity and conventionally estimated as the radius at which the mass density reaches a few hundred times the critical density ρ_c (e.g., Lahav et al. 1991), the turn-around radius is a linear quantity and not readily estimated from the physical properties of a bound object observed in the present epoch. In principle, the turn-around radius of a massive object could be determined as the distance to the "zero velocity surface" (e.g., Karachentsev et al. 2014) where the peculiar motion caused by the gravitational force of the given object cancels out the receding motion of the Hubble flow. But, the high degree of inaccuracy normally involved in the measurements of the peculiar velocity field (see Watkins & Feldman 2015, and references therein) has so far made it unfavored to use the turn-around radius as a cosmological probe.

Nevertheless, recently, Pavlidou & Tomaras (2014) recounted the advantages of using this classical concept as a test of the background cosmology. They first analytically proved the existence of a *time-independent direct* relation between the upper-limit of the turn-around radius and the density of dark energy, emphasizing the utmost utility of this relation as an invalidator of dark energy candidates including the standard cosmological constant Λ (see also Pavlidou et al. 2014). The other discriminative merit of the turn-around radius that Pavlidou & Tomaras (2014) pointed out is that it is not affected by complicated non-gravitational baryonic processes, which often obscure the powers of the standard diagnostics such as the redshift distortion effect, number counts of galaxy clusters, weak lensing effect and so on (see, e.g., Jing et al. 2006; Rudd et al. 2008; Balaguera-Antolínez & Porciani 2013; Hellwing et al. 2016).

In the wake of Pavlidou & Tomaras (2014), probing attention has been paid to the turn-around radius and its prospect for an independent test of dark energy and gravity. For instance, Faraoni (2016) have studied how the turn-around radius evolves in models with modified gravity (MG) and showed that a broad class of MG models could be ruled out through the measurements of the turn-around radii given its strong variation with the degree of MG. Tanoglidis et al. (2016) studied analytically the evolution of the turn-around

radius of a massive halo in a ΛCDM universe and found its sensitivity on the amount of dark energy. Lee et al. (2015) enhanced the feasibility of employing the turn-around radius as a cosmological diagnostics by putting forth a novel methodology to measure it in practice. Their methodology is based on the numerical finding of Falco et al. (2014) that the radial profile of the peculiar velocity field, $v_p(r)$, in the bound-zone around a massive object with virial mass $M_{\rm v}$ and radius $r_{\rm v}$ is well described by the following universal formula:

$$v_p(r) = -a \left(\frac{GM_{\rm v}}{r_{\rm v}}\right)^{1/2} \left(\frac{r_{\rm v}}{r}\right)^b , \tag{1}$$

where a and b are the amplitude and the slope parameters of the velocity profile, respectively, and r is the radial distance from the center of the object. Falco et al. (2014) demonstrated that in the bound zone corresponding to $3 \leq r/r_v \leq 8$, Equation (1) with constant values of $a \approx 0.8 \pm 0.2$ and $b \approx 0.42 \pm 0.16$ agrees very well with the numerically obtained profile from a high-resolution N-body experiment, no matter how massive the bound objects are.

Noting that at the turn-around radius (say, $r_{\rm t}$) Equation (1) should equal the velocity of the Hubble flow in magnitude, Lee et al. (2015) suggested that the value of $r_{\rm t}$ be found as a solution to $a\,(GM_{\rm v}/r_{\rm v})^{1/2}\,(r_{\rm v}/r_{\rm t})^b = H_0 r_{\rm t}$. In other words, using the new methodology developed by Lee et al. (2015) it is possible to estimate the turn-around radius of a massive object without having to measure the peculiar velocity field in the bound-zone as far as prior information on its viral mass is available. Lee et al. (2015) applied their methodology to a nearby isolated galaxy group, NGC5353/4 (Tully & Trentham 2008; Tully 2015), and discovered that the estimated turn-around radius of the group exceeds the upper limit derived by Pavlidou & Tomaras (2014) for a ΛCDM cosmology. Yet, before interpreting their result as a tension against the ΛCDM (Λ+Cold Dark Matter) paradigm, Lee et al. (2015) was emphatic about the need for further investigation of the validity of Equation (1) to which the success of their methodology was subject.

Given that Falco et al. (2014) derived the universal formula for $v_p(r)$ by measuring the peculiar velocities of *dark matter particles* located in the bound zone around the cluster-size halos, it should be important to examine whether or not the same formula also works for the case that $v_p(r)$ is determined from the peculiar velocity field of the bound-zone halos rather than that of dark matter particles since the latter is impossible to measure in practice. Moreover, it should be also quite necessary to explore more extensively if and how the peculiar velocity profile of the bound-zone halos evolve with redshifts. Although Falco et al. (2014) claimed that Equation (1) is universal with constant parameters, it may be true only for the case of the bound-zone dark matter particles but not for the case of the bound-zone halos, since it would take longer time for the halos to become stabilized in the bound-zone after their formation. If the peculiar velocity profile of the bound-zone halos turns out not to

be constant, then its evolution relation as a function of redshift might also exhibit a distinct dependence on the background cosmology. In this paper, we are to perform these follow-up tasks by measuring the peculiar velocity profile of the bound-zone objects around massive group-sized halos from the numerical data based on high-resolution N-body simulations.

2. PECULIAR VELOCITY PROFILES OF THE BOUND-ZONE OBJECTS

We utilize the Friends-of-Friends (FoF) halo catalogs produced by the Millennium-II simulations for a ΛCDM cosmology with $\Omega_m = 0.25,\ \Omega_\Lambda = 0.75,\ \Omega_b = 0.045,\ h = 0.73,\ \sigma_8 = 0.9,\ n_s = 1$ (Boylan-Kolchin et al. 2009). The simulations were performed with high resolution in a periodic box of volume $100^3\,h^{-3}\mathrm{Mpc}^3$ with 2160^3 DM particles each of which has equal mass of $6.885 \times 10^6\,h^{-1}M_\odot$. The Millennium-II simulations identified the DM halos by applying the FoF finder to each snapshot recorded at various redshifts. To have a full description of the Millennium-II N-body simulation and the FoF halo catalogs, refer to Lemson & Virgo Consortium (2006) and Boylan-Kolchin et al. (2009).

Various physical properties of each DM halo such as its mass (M_{200}), radius (r_{200}), number of its component DM particles, positions ($\mathbf{x}$) and peculiar velocities ($\mathbf{v}_p$) are provided in the Millennium-II halo catalog. Here r_{200} is the radius at which the mean mass density ρ equals 200 times the critical mass density ρ_c and M_{200} is the mass contained within a sphere with radius r_{200}, satisfying $M_{200} = (4\pi/3)(200\rho_\mathrm{c})r_{200}^3$. For our analysis throughout this paper, we regard r_{200} and M_{200} as the viral radius and viral mass, respectively.

We first make a sample of the group-sized halos by selecting those halos whose viral masses, M_g, exceed $10^{13}\,h^{-1}M_\odot$ from the Millennium-II halo catalogs. For each selected group-sized halo, we search for the bound zone halos which satisfy the following two conditions: First, the virial mass M_b of the bound-zone halos exceeds a certain threshold value, $M_\mathrm{b,c}$. To begin with, we set $M_\mathrm{b,c}$ at $10^8\,h^{-1}M_\odot$. Second, the radial distance, r, from the group center is in the range of $3 \le r/r_\mathrm{v} \le 8$ where r_v is the viral radius of the group (Falco et al. 2014). This range corresponds to the bound-zone where the peculiar velocity field can be treated as a linear quantity. The inner range $r/r_\mathrm{v} < 3$ is called the "infall zone" where the peculiar velocity field behaves nonlinearly, while the outer range $r/r_\mathrm{v} > 8$ is the "Hubble zone" where the peculiar velocity field is effectively zero (Zu et al. 2014; Lee et al. 2015). In our analysis, we focus only on the bound-zone peculiar velocity field.

Projecting the peculiar velocities of the bound-zone halos, $\mathbf{v}_p$, onto the radial direction toward the group center, we investigate how the rescaled value $\tilde{v}_p \equiv v_p/V_c$ with $V_c \equiv [(GM_\mathrm{v})/r_\mathrm{v}]^{1/2}$ changes as a function of the rescaled radial distance $\tilde{r} \equiv r/r_v$. From here

on, for simplicity, a group-sized halo in our sample ($M_{\rm g} \geq 10^{13}\,h^{-1}M_{\odot}$) is called a group and the magnitude of the component of the peculiar velocity of a bound-zone halo along the radial direction is called the bound-zone peculiar velocity, denoted by $v_{\rm p}(r)$. Note that the massive cluster-sized halos (say, $M_{\rm g} \geq 10^{14}\,h^{-1}M_{\odot}$) are included in our sample of the groups.

For each group, we bin the rescaled radial distance $\tilde{r}$ and count the numbers of the bound-zone halos, $N_{\rm b}$, whose radial distances belong to each bin. Let $\tilde{v}_p^{\alpha,\beta}$ denote the rescaled peculiar velocity of the α-th bound-zone halo around the β-th group at a given bin, $\tilde{r}$. The peculiar velocity profile of the bound-zone halos averaged over a total of $N_{\rm g}$ groups in our sample is evaluated as

$$\tilde{v}_p(\tilde{r}) = \frac{1}{N_{\rm g}} \sum_{\beta} \left[\frac{1}{N_{\rm b}} \sum_{\alpha} \tilde{v}_p^{\alpha,\beta}(\tilde{r}) \right] . \tag{2}$$

Figure 1 plots the resulting bound-zone peculiar velocity profile at $z = 0$ from the Millennium-II simulations as filled circular dots. Here, the errors $\sigma_{\rm v}$ are computed as the standard deviation in the measurements of the average value of $\tilde{v}_p(\tilde{r})$.

Now that the numerical result for $\tilde{v}_p(\tilde{r})$ has been obtained, we fit it to the analytic model, Equation (1), by adjusting the amplitude and slope parameters, a and b, with the help of the maximum likelihood method. Basically, we search for (a, b) which maximizes the joint probability, $p(a, b) \propto \exp\left[-\chi^2(a, b)/2\right]$, where the *reduced* chi-square $\chi^2(a, b)$ is given as

$$\chi^2_{\nu}(a, b) = \frac{1}{(N_{\rm bin} - 2)} \sum_{i=1}^{N_{\rm bin}} \frac{\left[\tilde{v}_p(\tilde{r}_i) - \tilde{v}^2_{\rm p,model}(\tilde{r}_i; a, b)\right]^2}{\sigma^2_{\rm v}(\tilde{r}_i)} , \tag{3}$$

where $N_{\rm bin}$ is the number of the bins of the rescaled radial distance $\tilde{r}$, $\tilde{v}_p(\tilde{r}_i)$ denotes the value of the numerically obtained peculiar velocity profile of the bound zone halos at the i-th bin $\tilde{r}_i$, while $\tilde{v}_{\rm p,model}(\tilde{r}_i; a, b)$ represents the analytic prediction of Equation (1) at $\tilde{r}_i$ where the amplitude and slope parameters have the values of a and b, respectively. Since the analytic model has two adjustable parameters, the degree of freedom for the chi-square equals $N_{\rm bin} - 2$ (Wall & Jenkins 2012).

In Figure 1 the fitting model with the best parameter values of a and b is shown as red solid line. Although the overall accord between the numerical and the fitting results is quite good, the numerical value, $\tilde{v}_p(\tilde{r}_i)$ at the left-most bin appears to depart from the overall trend. That is, the numerical result shows a bit flatter shape than the analytic model in the lowest $\tilde{r}$ bin. We suspect that it is because in the boundary, $\tilde{r} \approx 3$, between the infall and the bound zones, the nonlinear aspect of the gravitational force of a group begins to be effective, leading to a departure of the peculiar velocity from the linear behavior at $r \approx 3r_{\rm v}$. To remove this contamination caused by the nonlinear effect from the construction

of the bound-zone peculiar velocity profile, we exclude the left-most bin from the procedure and reperform the fitting over the narrower range of $3.5 \leq \tilde{r} \leq 8$, the result of which is shown as blue solid line in Figure 1. As can be seen, the narrower range yields a better fit to the numerical result. The excellent match between the numerically obtained profile and Equation (1) confirms the validity of the analytic formula of Falco et al. (2014) even for the case that the bound-zone peculiar velocity profile is constructed not from DM particles but from the halos.

Figure 2 plots the $1\sigma,\ 2\sigma,\ 3\sigma$ contours of $p(a, b)$ at $z = 0$ in the a-b plane as the thickest, thick and thin solid lines, respectively, under the assumption that the joint probability density distribution $p(a, b)$ is well approximated as a multi-variate Gaussian distribution. Here, the $1\sigma,\ 2\sigma$ and 3σ contours show the areas in the a-b plane over which the probability, $\int da \int db\, p(a, b)$, has the values of 0.68, 0.95 and 0.99, respectively. To compute the errors associated with the measurements of the best-fit values of a and b, we first marginalize the joint probability density $p(a, b)$ to evaluate the probability density distributions of the two parameters, $p(a)$ and $p(b)$, as $p(a) = \int db\, p(a, b)$ and $p(b) = \int da\, p(a, b)$, the results of which are displayed as black solid lines in Figures 3 and 4, respectively. As can be seen, both of $p(a)$ and $p(b)$ are nearly symmetric about the values at which the probability densities reach the highest values. The marginalized errors associated with the measurements of the best-fit parameters are calculated as $\int_{a_{\rm max}}^{a_{\rm max}+\sigma_{a+}} da\, p(a) = 0.34$, $\int_{a_{\rm max}-\sigma_{a-}}^{a_{\rm max}} da\, p(a) = 0.34$, $\int_{b_{\rm max}}^{b_{\rm max}+\sigma_{b+}} db\, p(b) = 0.34$, $\int_{b_{\rm max}-\sigma_{b-}}^{b_{\rm max}} db\, p(b) = 0.34$, where $a_{\rm max}$ and $b_{\rm max}$ represent the most probable values of a and b.

The first row of Table 1 lists the number of the groups ($N_{\rm g}$), the total number of the bound-zone halos ($N_{\rm T,b}$), the best-fit values of the amplitude and slope parameters (a and b), and the minimum value of the reduced chi-square, $\chi^2_\nu \equiv \chi^2/(N_{\rm bin} - 2)$ at $z = 0$. Note that the best-fit ranges of the two parameters, $a = 0.74 \pm 0.03$ and $b = 0.38 \pm 0.03$ found in the current work are well overlapped with those found in the original work of Falco et al. (2014), $a = 0.8 \pm 0.2$ and $b = 0.42 \pm 0.16$. This result implies that the bound-zone peculiar velocity profile constructed from the bound-zone halos can be described by the same analytic formula, Equation (1) with the same parameters , that Falco et al. (2014) originally derived from the bound-zone DM particles. As mentioned in Section 1, the bound-zone peculiar velocity profile can be reconstructed only from the bound objects in real observations, this result holds up the reliability and practicality of the analytic formula of Falco et al. (2014).

Recall that for the numerical simulations utilized by Falco et al. (2014) the normalization amplitude of the initial power spectrum was set at $\sigma_8 = 0.76$ (Spergel et al. 2007), substantially different from the value of $\sigma_8 = 0.9$ adopted for the Millennium-II simulations (Boylan-Kolchin et al. 2009). Recall also that in the original work of Falco et al. (2014) the

ratio of the mass overdensity within the virial radius to ρ_c was set at $\Delta = 97.8$ while in the current work based on the Millennium-II simulations it is $\Delta = 200$. In spite of these differences, the best-fit values of the amplitude and slope of the bound-zone peculiar velocity profile obtained in our fitting procedure agree quite well with the original values determined Falco et al. (2014). This result implies that the analytic formula of the bound-zone peculiar velocity profile with constant amplitude and slope should be insensitive to the key cosmological parameter values as well as to the details of the way in which the virial radius/mass is defined. However, before concluding that the bound-zone peculiar velocity profile is truly universal, a further investigation should be performed about the constancy of its amplitude and slope against the change of redshifts.

3. EVOLUTION OF THE BOUND-ZONE PECULIAR VELOCITY PROFILES

We refollow the whole procedures arranged in Section 2 with the halos identified at higher redshifts: selecting the groups with virial mass $M_g \geq 10^{13}\,h^{-1}\,M_\odot$; searching for the bound-zone halos at $3 \leq \tilde{r} \leq 8$ with virial mass $M_b \geq 10^8\,h^{-1}\,M_\odot$; constructing the peculiar velocity profile of the bound-zone halos $\tilde{v}_p$ as a function of $\tilde{r}$; fitting $\tilde{v}_p$ to Equation (1) and determine the best-fit parameters, (a, b), that minimize χ^2 given in Equation (3) or equivalently maximizes $p(-\chi^2/2)$. Figure 5 shows the numerical results (filled circular dots with errors) along with the best-fit models (red solid lines) at nine different redshifts in the range of $0.1 \leq z < 1$. It is obvious that the fitting formula, Equation (1), is indeed as successful at higher redshifts as at the present epoch in matching the numerical results. Unlike the case of $z = 0$, we do not find a departure of the numerical data point from the overall trend in the left-most bin, $\tilde{r} = 3$, at $z \geq 0.1$ and thus use the whole range of $3 \leq \tilde{r} \leq 8$ without excluding the left-most bin. This phenomenon indicates that the nonlinear effect on the peculiar velocity field in the boundary ($\tilde{r} = 3$) between the infall and the bound zones becomes significant only at the present epoch.

Figure 6 show the same as Figure 2 but at nine different epochs. As can be seen, at earlier epochs the peculiar velocity profiles of the bound-zone halos are characterized by lower amplitudes and lower slopes. To see more explicitly how the amplitude and slope of the peculiar velocity profile of the bound-zone halos change with redshift, we plot the best-fit values of a and b versus z in Figure 7. In the high-z section ($z > 0.6$), the best-fit amplitude and slope appear to be uniform, independent of z. In the intermediate-z section ($0.2 \leq z \leq 0.6$), the best-fit parameters vary with z, making a gradual transition toward higher values. In the low-z section ($z < 0.2$), the two parameters reexhibit uniformity, being

constant but at higher values than those in the high-z section ($z > 0.6$).

Noting in Figure 6 that the transitions of a and b to higher values start at the epoch when Λ begins to dominate the energy density of the universe, we ascribe the redshift-evolution of the bound-zone peculiar velocity profile to the effect of Λ. The higher slope of the bound-zone peculiar velocity profile in the low-z section can be understood as follows. The stronger repulsive force of the accelerating space-time after the onset of Λ would lead the peculiar velocities of the bound-zone halos to decrease more rapidly in magnitude with the radial distance. To understand the higher amplitude of the bound-zone peculiar velocity profile at $z \leq 0.6$, one has to recall that the amplitude, a, is proportional to the linearly extrapolated value of $v_p(r)$ to the viral radius, $r_{\rm v}$. For the gravitational force to resist the repulsive force of the accelerating space-time at the viral radius in the Λ-dominated epoch, it has to have a higher value, which yields higher amplitude of $v_p(r_{\rm v})$.

To see if this trend is robust against the change of the mass cut-off scale of the bound-zone halos, we impose a higher mass cut on the virial masses $M_{\rm b}$ of the bound-zone halos and repeat the whole process. Figure 8 shows the evolution of the amplitude and slope of the bound-zone peculiar velocity profiles for three different cases of the cuts imposed in the masses of the bound-zone halos. As can be seen, the three cases show the same trend. The amplitude and slope of the bound-zone peculiar velocity profile are constant when either DM or Λ dominates but evolving linearly with z when the energy density of Λ is comparable to that of DM. Despite that there is an order of magnitude change in the mass cut-off scales of the bound-zone halos, there is no substantial change in the best-fit values of a and b in the whole redshift range of $0 \leq z \leq 1$, which implies that the analytic formula of the bound-zone peculiar velocity profile is indeed robust against the variation of the mass cut-off scale of the bound-zone halos. Given that what can be measured accurately from observations is usually the properties of the luminous massive galaxies but not those of the low-mass dwarf galaxies, our results offers a good prospect for the practical application of the bound-zone peculiar velocity profile in real observations.

4. SUMMARY AND DISCUSSION

This work is a follow-up to Lee et al. (2015) who proposed a new methodology to estimate the turn-around radius of a bound object without resorting to the inaccurate measurements of the peculiar velocity field. Applying their methodology to the bound-zone galaxies of the NGC 5353/4 group, Lee et al. (2015) have found that the turn-around radius of the group exceeds the upper limit set by the standard ΛCDM cosmology. Since the success of the methodology of Lee et al. (2015) was contingent upon the validity of the analytic

formula derived by Falco et al. (2014) for the bound-zone peculiar velocity profile, it was required to test extensively the robustness of the formula before interpreting the estimated turn-around radius of the NGC 5353/4 group as a counter-evidence against the ΛCDM cosmology. In the current work, we have performed the required test by utilizing the high-resolution Millennium-II simulations (Boylan-Kolchin et al. 2009). First, we have examined if the same analytic formula is also applicable to the case that the peculiar velocities were measured not from individual DM particles but from the bound-zone galaxies or halos. We have also investigated if the bound-zone peculiar velocity profile is truely universal, being well described by the same redshift-independent formula, as claimed by Falco et al. (2014).

Analyzing the halo catalogs in the redshift range of $0 \leq z \leq 1$ produced by the Millennium-II simulations (Boylan-Kolchin et al. 2009), we have constructed the peculiar velocity profiles of the bound-zone halos with mass $M_{\rm b} \geq 10^8\,h^{-1}\,M_\odot$ around massive group-size halos with mass $M_{\rm g} \geq 10^{13}\,h^{-1}\,M_\odot$ and determined the amplitude and slope of the bound-zone peculiar velocity profile by comparing the formula to the numerical results. We have shown that the peculiar velocity profile of the bound-zone halos can be well approximated by the same analytic model of Falco et al. (2014), even when the profile is constructed not from dark matter but from the halos. However, it has been found that the amplitude and slope parameters, a and b, of the bound-zone peculiar velocity profile do not show perfect constancy but evolve with redshifts: In the high redshift range $0.6 < z \leq 1$, the two parameters are found to have constant values around $a = 0.53$ and $b = 0.28$. In the intermediate redshift range $0.2 \leq z \leq 0.6$, both of the two parameters increase almost linearly with the decrement of z. In the low redshift range $z \leq 0.2$ the constancy of the two parameters is recovered and the best-fit values of a and b are found to agree fairly well with the original values of $a = 0.42$ and $b = 0.8$ determined by Falco et al. (2014).

Noting the coincidence between the epoch when the redshift evolution of the two parameters starts and the epoch when the density of Λ, ρ_Λ, begins to exceed that of dark matter, $\rho_{\rm m}$, in the universe, we have claimed that the growing effect of Λ should be responsible for the variation of the amplitude and slope of the bound-zone peculiar velocity profile in the intermediate redshift range $0.2 \leq z \leq 0.6$. We have explained that the accelerating space-time in the Λ-dominated era has an effect of steepening the peculiar velocity profile and reducing the circular velocity by defeating more drastically the gravitational attraction of massive halos with the increment of the radial distances.

We have also verified that the bound-zone peculiar velocity profile is robust against the variation of the initial conditions of the ΛCDM universe, demonstrating that in spite of the different values of the key cosmological parameters adopted by the Millennium-II simulations from that of Falco et al. (2014) the best-fit values of the amplitude and slope

parameters of the bound-zone peculiar velocity profile determined by our analysis agree well the original values found by Falco et al. (2014). Along with our another finding that the bound-zone peculiar velocity profile is also robust against the variation of the mass cut-off scale of the bound-zone objects, our results altogether lead us to the bottom line that in the low-redshift range $z \leq 0.2$ when the Λ-domination prevails the bound-zone peculiar velocity profile is indeed universal, providing a compelling numerical evidence for the original claim of Falco et al. (2014).

We speculate that the length of the transition period when the amplitude and slope parameters of the bound-zone peculiar velocity profile grow linearly with the decrement of redshifts should be a powerful estimator of the amount of Λ in the *local* universe, since it depends sensitively when the Λ-domination starts and prevails. We also speculate that the linear growth of the amplitude and slope parameters of the bound-zone peculiar velocity profile during the transition period of $0.2 \leq z \leq 0.6$ may be a unique signature of the ΛCDM cosmology: In alternative dark energy models or in MG models, the growth rate would deviate from being constant and might assume a dependence on the redshift, given that it reflects how rapidly the acceleration of spacetime cracks the balance between the gravity and the Hubble expansion. It might be possible to distinguish between alternative cosmologies by measuring the growth rate of the amplitude and slope of the bound-zone peculiar velocity profile during the transition period from observations. Of course, what should precede is to investigate quantitatively at what rates the characteristic parameters of the bound-zone peculiar velocity profile grow in alternative models. Our future work is in this direction.

We thank an anonymous referee for very helpful comments. This work was supported by a research grant from the National Research Foundation (NRF) of Korea to the Center for Galaxy Evolution Research (NO. 2010-0027910) and partially by the support of the Basic Science Research Program through the NRF of Korea funded by the Ministry of Education (NO. 2013004372). The Millennium-II Simulation databases used in this paper and the web application providing online access to them were constructed as part of the activities of the German Astrophysical Virtual Observatory (GAVO).

REFERENCES

Balaguera-Antolínez, A., & Porciani, C. 2013, JCAP, 4, 022

Barrow, J. D., & Saich, P. 1993, MNRAS, 262, 717

Boylan-Kolchin, M., Springel, V., White, S. D. M., Jenkins, A., & Lemson, G. 2009, MNRAS, 398, 1150

Borisov, A., Jain, B., & Zhang, P. 2012, Phys. Rev. D, 85, 063518

Brooks, A. M., & Zolotov, A. 2014, ApJ, 786, 87

Falco, M., Hansen, S. H., Wojtak, R., et al. 2014, MNRAS, 442, 1887

Fan, Y., Wu, P., & Yu, H. 2015, Phys. Rev. D, 92, 083529

Faraoni, V. 2016, Physics of the Dark Universe, 11, 11

Gunn, J. E., & Gott, J. R., III 1972, ApJ, 176, 1

Hellwing, W. A., Schaller, M., Frenk, C. S., et al. 2016, arXiv:1603.03328

Karachentsev, I. D., Tully, R. B., Wu, P.-F., Shaya, E. J., & Dolphin, A. E. 2014, ApJ, 782, 4

Jing, Y. P., Zhang, P., Lin, W. P., Gao, L., & Springel, V. 2006, ApJ, 640, L119

Lahav, O., Lilje, P. B., Primack, J. R., & Rees, M. J. 1991, MNRAS, 251, 128

Lee, J., Kim, S., & Rey, S.-C. 2015b, ApJ, 815, 43

Lemson, G., & Virgo Consortium, t. 2006, arXiv:astro-ph/0608019

Mota, D. F., & van de Bruck, C. 2004, A&A, 421, 71

Pavlidou, V., Tetradis, N., & Tomaras, T. N. 2014, JCAP, 5, 017

Pavlidou, V., & Tomaras, T. N. 2014, JCAP, 9, 020

Rudd, D. H., Zentner, A. R., & Kravtsov, A. V. 2008, ApJ, 672, 19-32

Spergel, D. N., Bean, R., Doré, O., et al. 2007, ApJS, 170, 377

Tanoglidis, D., Pavlidou, V., & Tomaras, T. 2016, arXiv:1601.03740

Tully, R. B., & Trentham, N. 2008, AJ, 135, 1488

Tully, R. B. 2015, AJ, 149, 54

Wall, J. V., & Jenkins, C. R. 2012, Practical Statistics for Astronomers, (Cambridge, UK: Cambridge University Press)

Watkins, R., & Feldman, H. A. 2015, MNRAS, 450, 1868

Zu, Y., Weinberg, D. H., Jennings, E., Li, B., & Wyman, M. 2014, MNRAS, 445, 1885

This preprint was prepared with the AAS LaTeX macros v5.2.

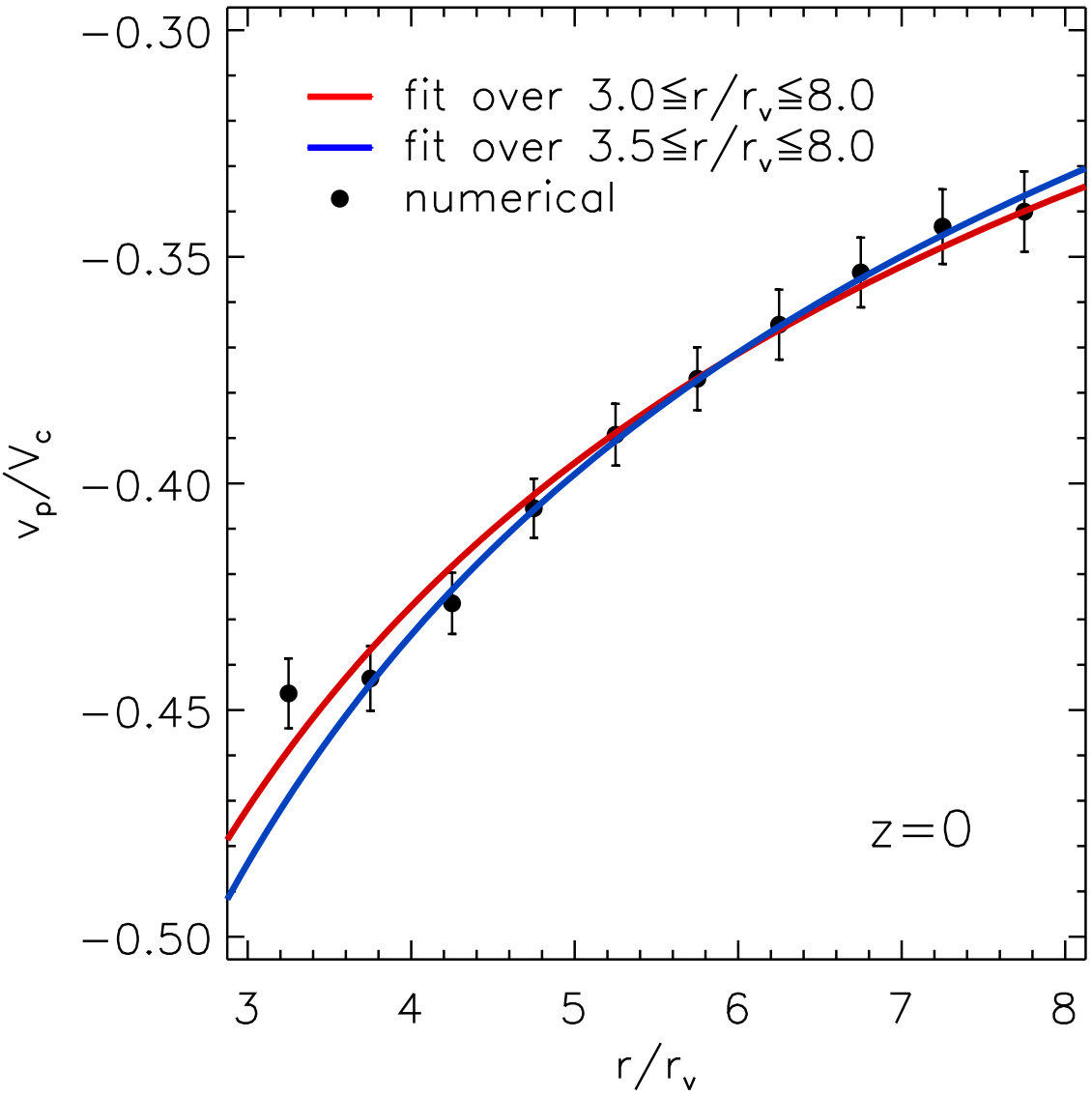

Fig. 1.— Peculiar velocity profile of the bound-zone halos with virial masses $M_{\rm b} \geq 10^8\,h^{-1}\,M_\odot$ around the groups with viral mass $M_{\rm g} \geq 10^{13}\,h^{-1}\,M_\odot$ at $z = 0$. The black filled circles with error bars are the numerical results from the Millennium II simulations, while the red and the blue solid lines represent the best-fit models over the range of $3 \leq r/r_{\rm v} \leq 8$ and $3.5 \leq r/r_{\rm v} \leq 8$, respectively.

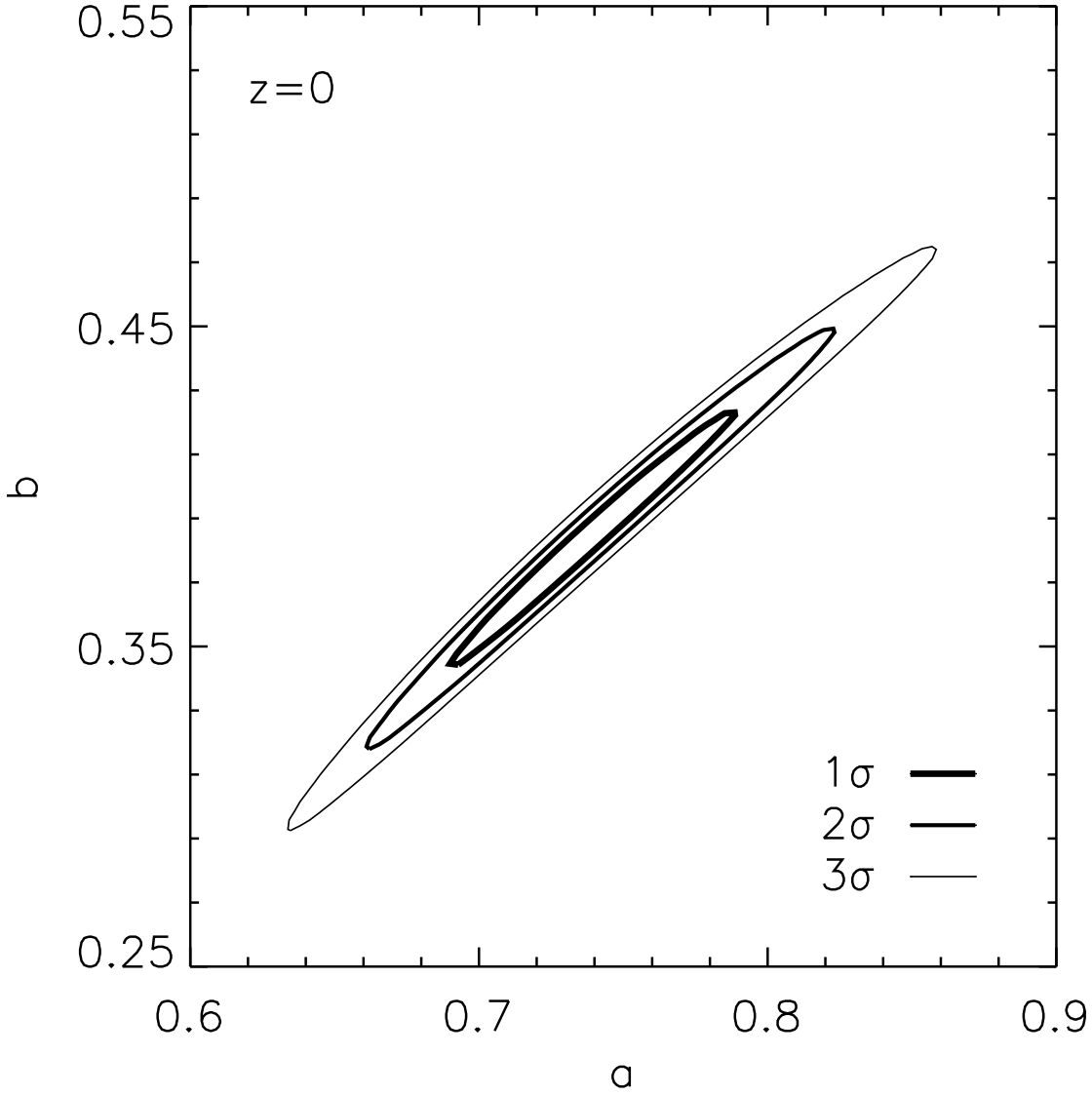

Fig. 2.— 1σ, 2σ and 3σ contours of χ^2 (thick, thin and the thinnest solid lines, respectively) in the a-b plane.

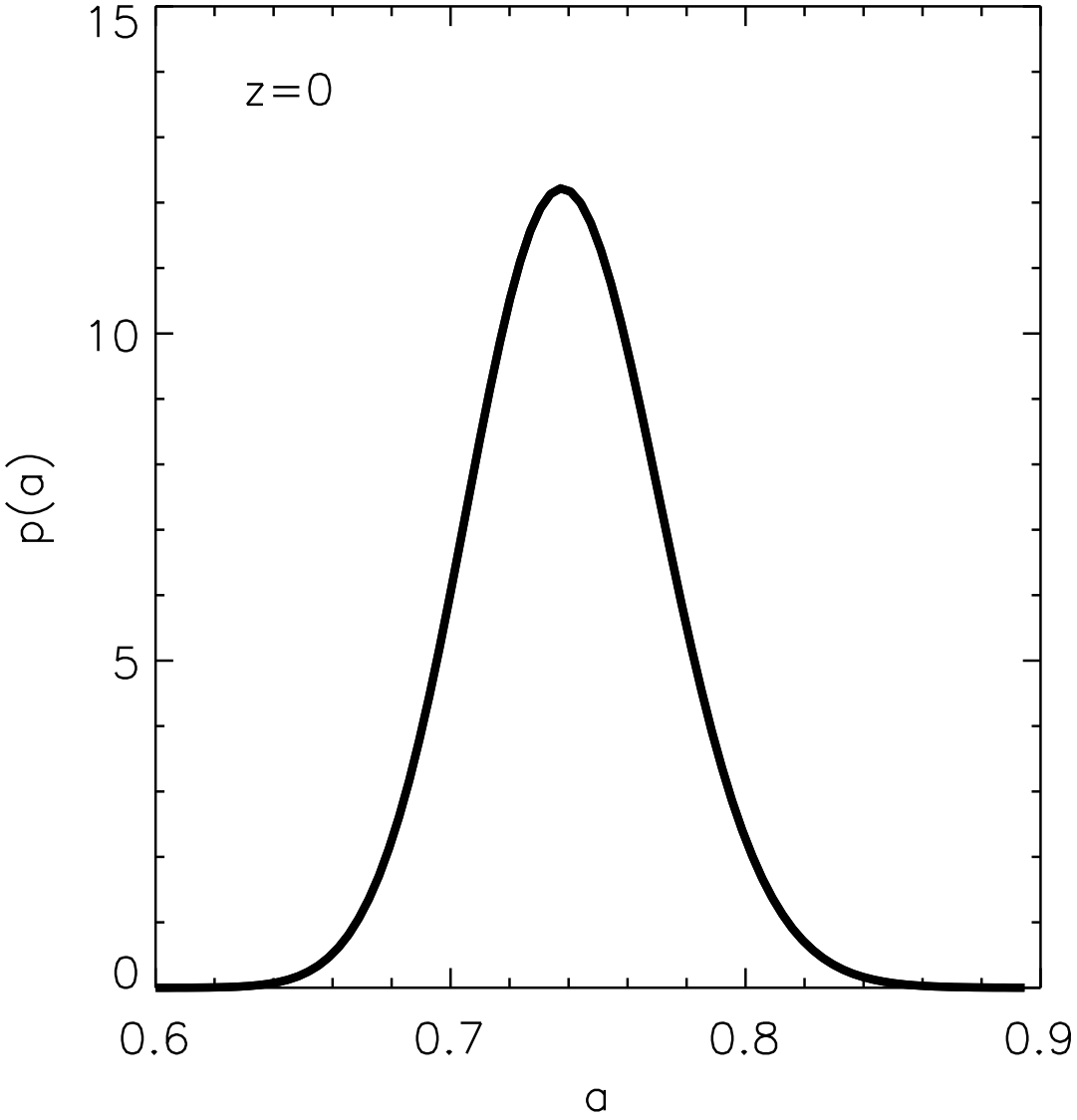

Fig. 3.— Probability density distribution of the amplitude parameter a obtained by marginalizing the joint probability density distribution over the slope parameter b at $z = 0$.

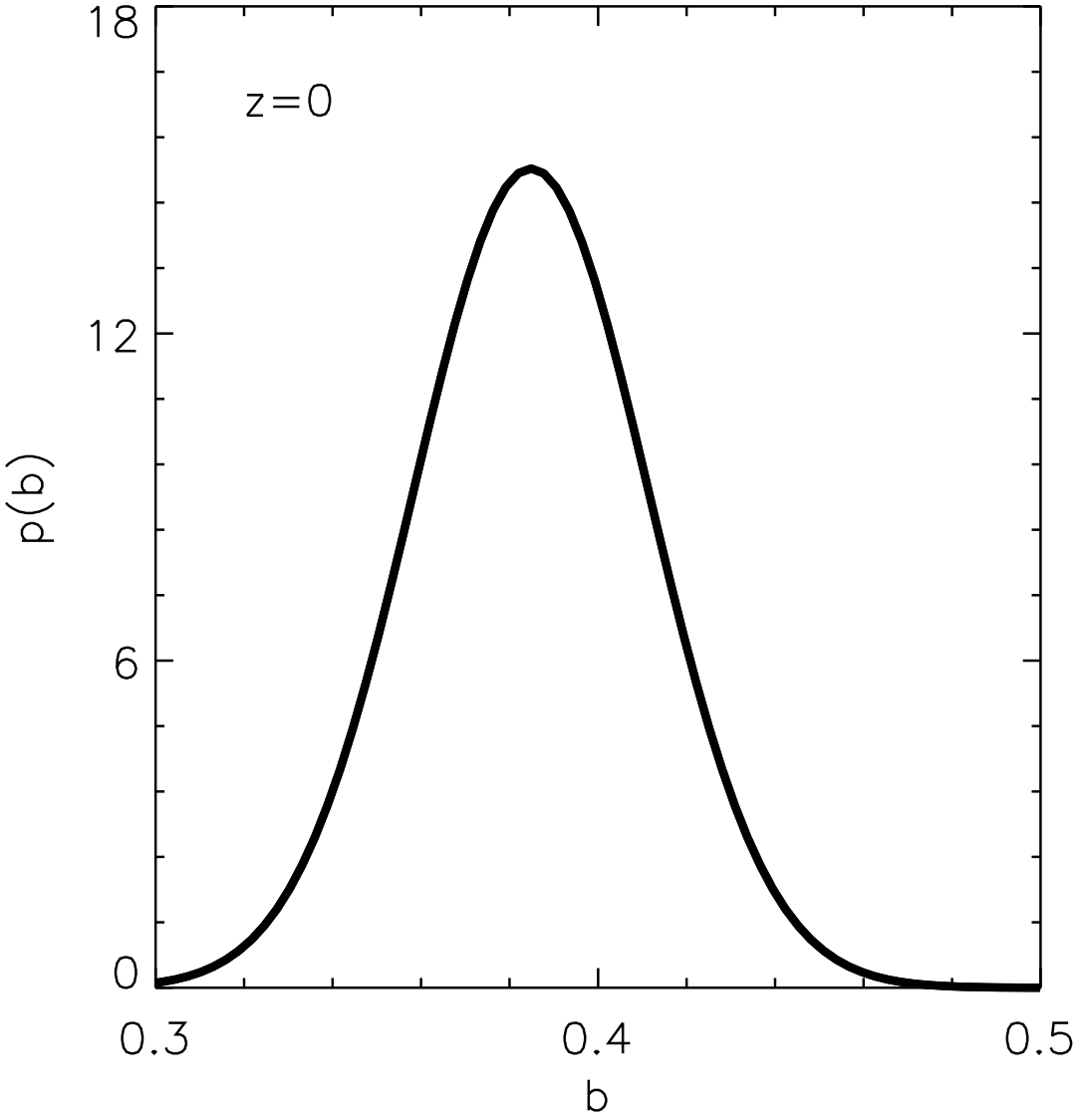

Fig. 4.— Probability density distribution of the slope parameter b obtained by marginalizing the joint probability density distribution over the amplitude parameter a at $z = 0$.

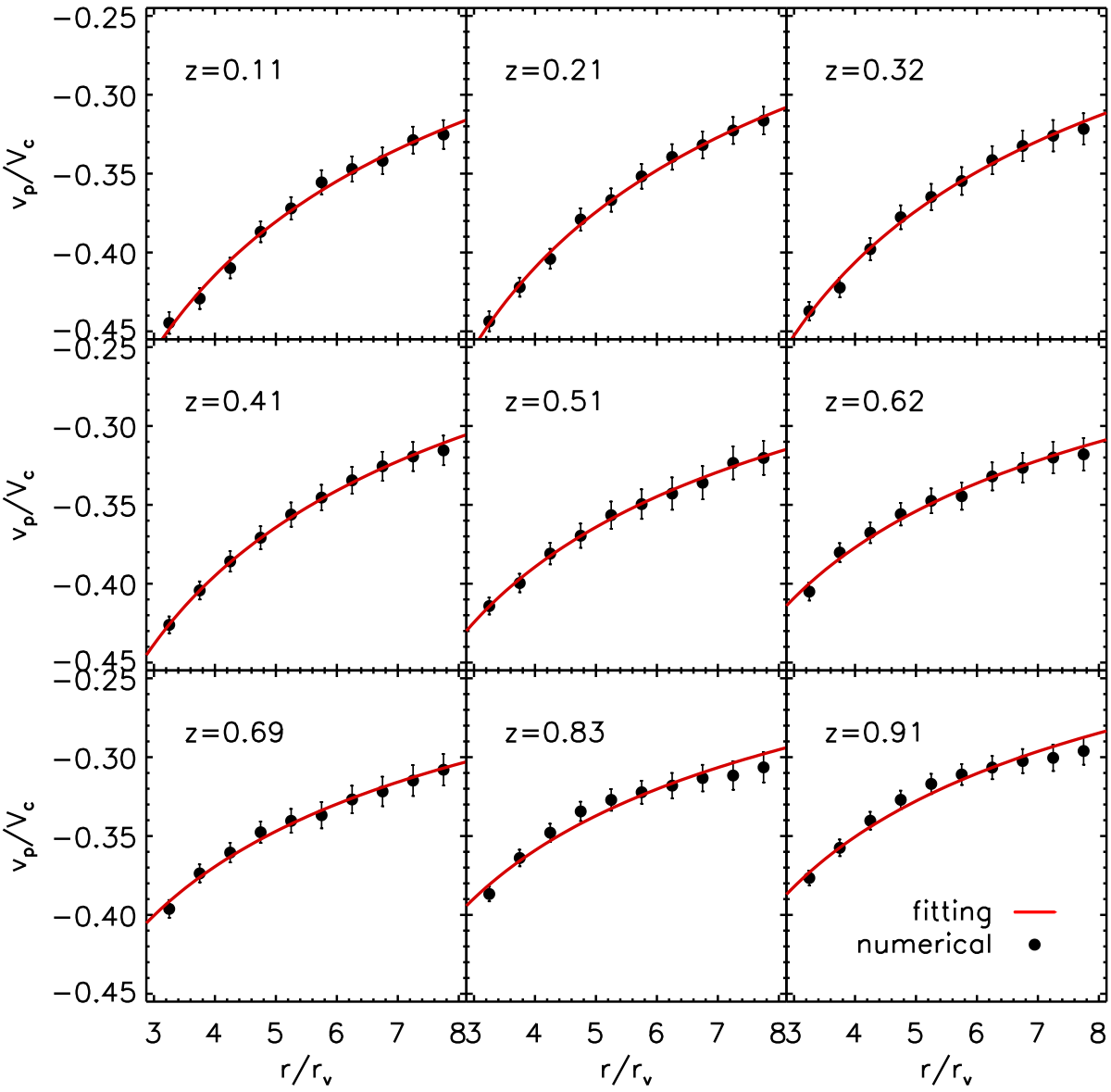

Fig. 5.— Peculiar velocity profiles of the bound-zone halos at nine different redshifts. In each panel the filled black circles with errors and the red solid lines represent the numerical results and the best-fit model, respectively.

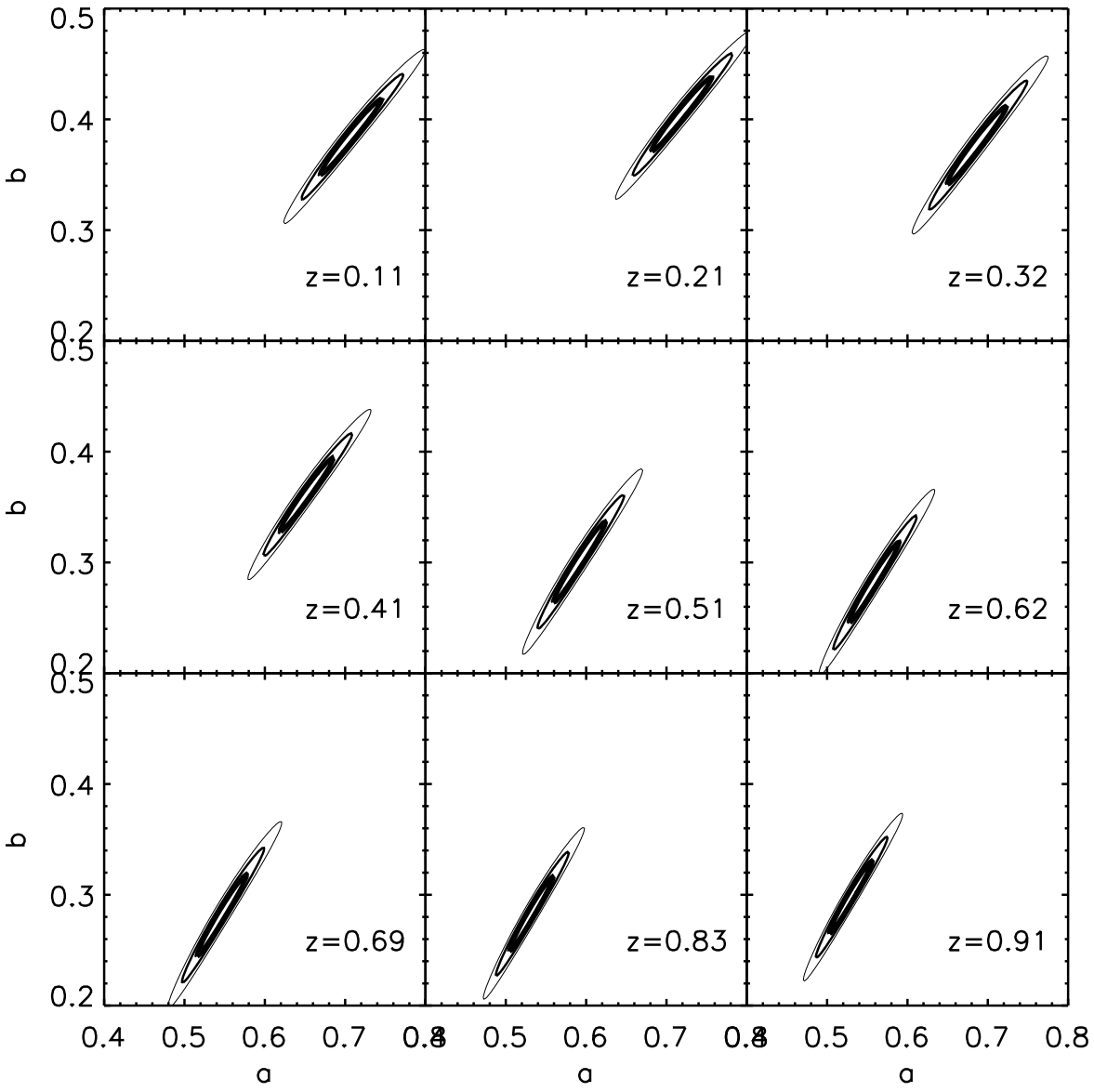

Fig. 6.— Same as Figure 6 but at nine higher redshifts.

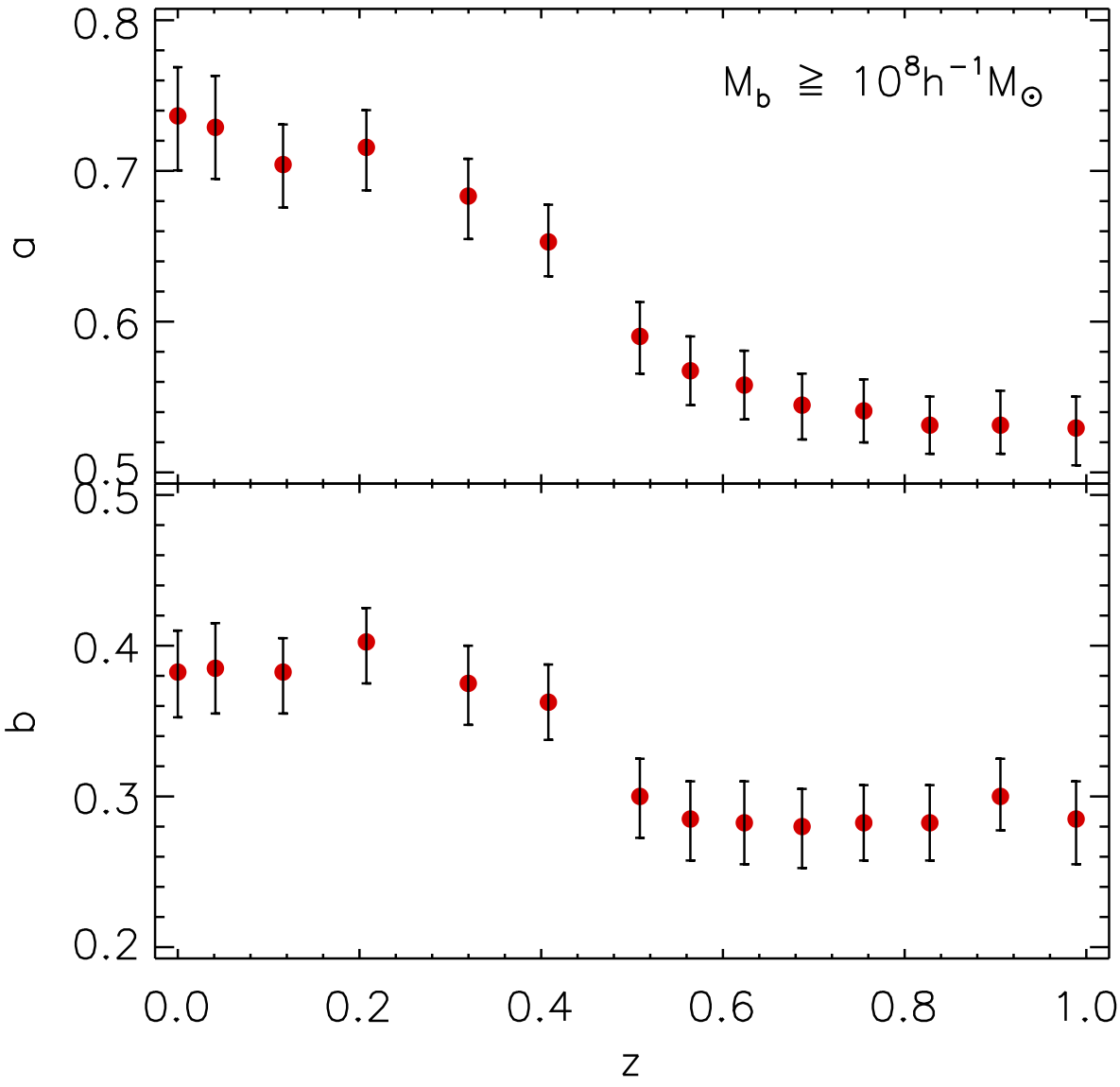

Fig. 7.— Variation of the best-fit parameters, a and b, in Equation (1) with redshifts in the top and bottom panels.

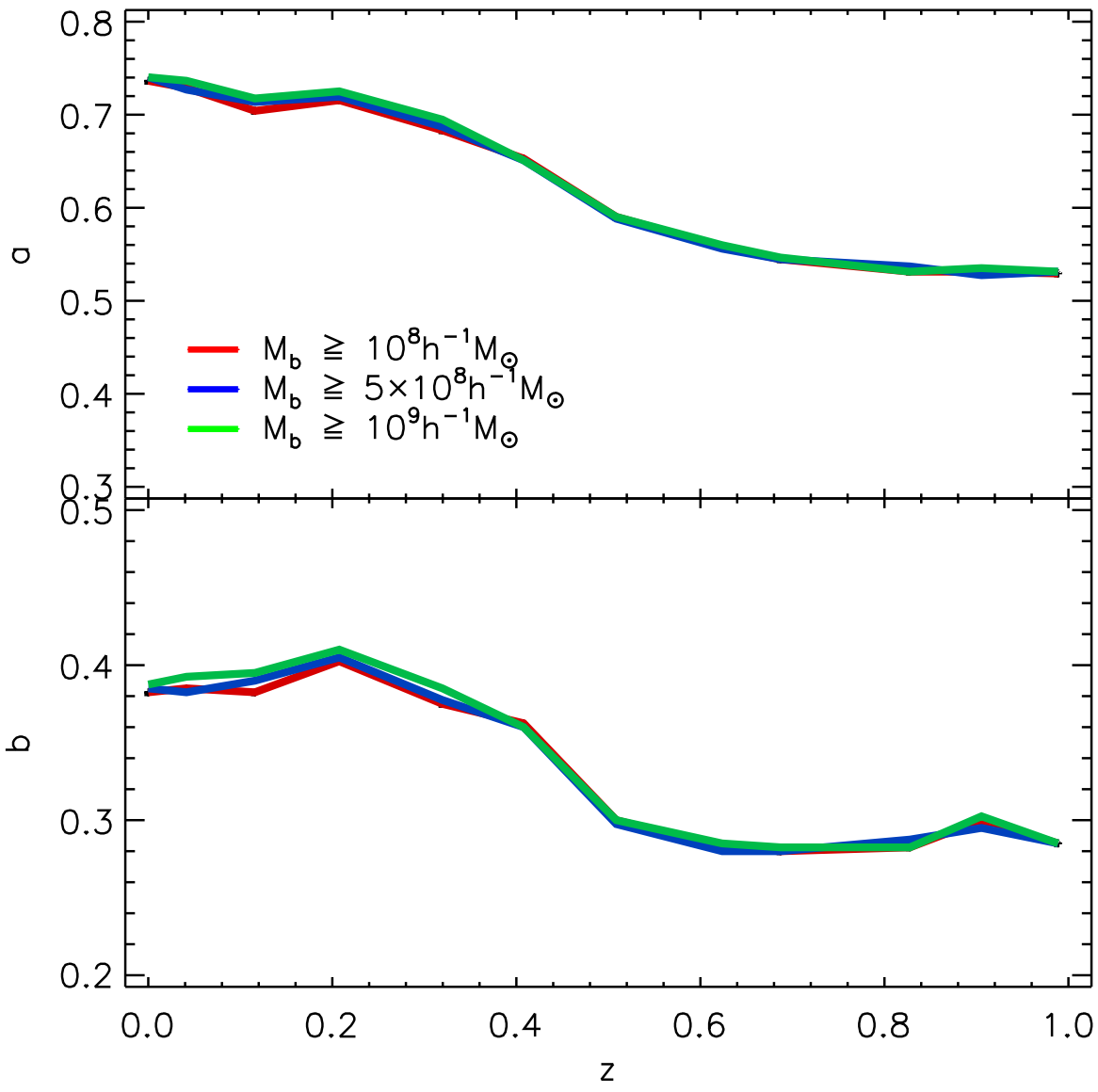

Fig. 8.— Same as Figure 7 but for three different cases of the cuts imposed on the virial masses of the bound-zone halos.

Table 1. Redshifts, number of the groups, number of the bound-zone halos around the groups, best-fit values of the amplitude and slope parameters of the bound-zone peculiar velocity profile with marginalized errors, and the reduced chi-square value for the case of $M_{\rm b} \geq 10^8\,h^{-1}\,M_\odot$.

z	$N_{\rm g}$	$N_{\rm T,b}$	a	b	χ^2_ν
0	301	604069	0.73 ± 0.03	0.38 ± 0.03	0.11
0.11	297	674335	0.70 ± 0.03	0.38 ± 0.02	0.28
0.21	282	691961	0.72 ± 0.02	0.40 ± 0.02	0.13
0.32	279	751384	0.68 ± 0.03	0.38 ± 0.03	0.20
0.41	271	797699	0.65 ± 0.02	0.36 ± 0.03	0.05
0.51	279	838630	0.60 ± 0.02	0.30 ± 0.03	0.06
0.62	257	828457	0.56 ± 0.02	0.28 ± 0.03	0.28
0.69	248	813384	0.54 ± 0.02	0.28 ± 0.03	0.23
0.83	222	750696	0.53 ± 0.02	0.28 ± 0.03	0.83
0.91	208	689159	0.53 ± 0.02	0.30 ± 0.03	0.64
0.99	203	691205	0.53 ± 0.02	0.28 ± 0.03	0.33